Improving single-photon sources with Stark tuning

Mark J. Fernée, Halina Rubinsztein-Dunlop, and G. J. Milburn

Center for Quantum Computer Technology, The University of Queensland, Queensland 4072, Australia

(Received 30 August 2006; published 25 April 2007)

We investigate the use of the Stark shift in atomlike systems in order to control the interaction with a high-Q/V microcavity. By applying a Stark shift pulse to a single atomlike system, in order to affect and control its detuning from a cavity resonance, the cavity QED interaction can be carefully controlled so as to allow stochastic pumping of the emitting state without causing random timing jitter in the output photon. Using a quantum trajectory approach, we conduct simulations that show this technique is capable of producing indistinguishable single photons that exhibit complete Hong-Ou-Mandel interference. Furthermore, Stark tuning control allows for the generation of arbitrary pulse envelopes. We demonstrate this by showing that a simple asymmetric Stark shifting pulse can lead to the emission of symmetric Gaussian single-photon pulse envelopes, rather than the usual exponential decay. These Gaussian pulses also exhibit complete Hong-Ou-Mandel interference. The use of Stark shifting in solid-state systems could ultimately provide the cheap miniature high quality single-photon sources that are currently required for applications such as all-optical quantum computing.

INTRODUCTION

All optical quantum computing [1] is a promising candidate for a scalable computing architecture. A number of major milestones have already been achieved [2–4]. Optical techniques for quantum control and manipulation may also play a role in other possible quantum technologies. However, there are a number of hurdles that remain before these technologies can be realized or implemented. One of the hurdles concerns the sources of photons for such technologies. There are stringent requirements on the quality of the single photons if they are to be used in these quantum technologies [5]. The most useful property is indistinguishability, which is readily measured using a Hong-Ou-Mandel (HOM) interferometer [6]. This property essentially implies that the same quantum process was used to generate each photon. This can be difficult to achieve in practice. Even if it is overcome, another common source of reduced contrast in the HOM interferometer comes from timing jitter [7]. For example, a single quantum dot emitter is usually pumped incoherently to a higher excited state and stochastically relaxes the emitting state. This stochastic relaxation process results in random population of the emitting state, which manifests as a timing jitter in the emitted photon. This in turn limits the level of interference that can be obtained with the HOM interferometer and introduces a random phase into the circuit. The best current technology which overcomes this problem is still the original scheme employed by Hong, Ou, and Mandel for generating two correlated photons using a spontaneous parametric down conversion process [6]. However, this technology brings its own problems, as the spontaneous nature means that the emission of the photon pair is random. This can provide synchronization problems for large networks of such sources, which require further technologies, such as photon memories [8,9], if it is to be implemented. The other option is to use a coherently driven source [10–14], such that the population of the emitting state is carefully controlled by a coherent driving laser. These sources have the advantage

that they can produce photon wave packets of arbitrary shape as well as being indistinguishable [12,13]. However, these sources invariably involve atomic emitters and must thus comprise a vacuum chamber and trapping apparatus. Therefore it is not expected that these sources will ever be suitable for use outside a laboratory environment.

It is expected that one of the most promising technologies would be based on a solid-state approach [15,16]. This allows for various implementations of cavity QED based systems, which facilitate efficient collection of photons. The atomiclike emitter can comprise either a quantum dot [15–17], single dopant ion, or a color center [18,19]. This provides a wide range of material properties that can be used to select the appropriate emission wavelength, lifetime, and decoherence properties. The current state of the art using these methods comprises a permanently coupled emitter-cavity system [16,20]. These systems have achieved some impressive results. However, they suffer the timing jitter problem that arises from stochastic population of the emitting state. As a result, two-photon HOM interference is usually compromised in such systems [7]. The photon pulse envelope is also fixed in these systems and determined by the cavity emission properties. In some prospective technologies, such as quantum memories [8,9], a more symmetrical pulse shape is desired.

In this paper, we look at controlling the detuning of a quantum emitter from a high-Q/V microcavity in order to remove timing jitter from the emission process. This is accomplished using Stark tuning with an electric field. The use of a high Q/V microcavity ensures that the photon is emitted into a single mode with high efficiency as well as ensuring that the required Stark shifting field is not too great. We also show that by carefully choosing the Stark shifting pulse shape, the output photon pulse envelope can be modified. This is demonstrated by showing that high quality single photons with a Gaussian pulse envelope are possible using a straightforward modification of the Stark pulse shape.
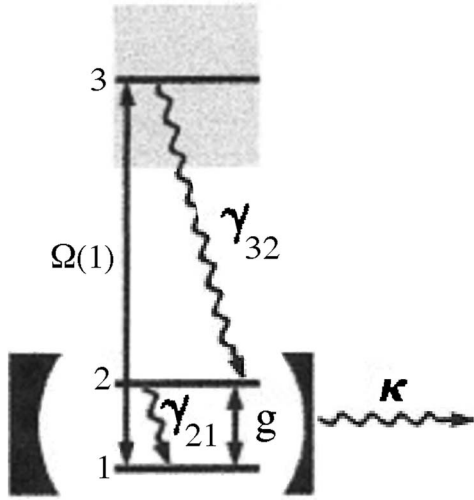
FIG. 1. Diagram of the three-level system with the lower two levels interacting with a single cavity mode. The upper level is shaded to represent a manifold of states in the solid-state environment, which nonradiatively relax to the state $|2\rangle$. The relaxation rates γ_{ij} represent loss to various reservoirs. The term $\Omega(t)$ is the coherent pumping pulse and g represents the field-atom coupling constant. The rate of loss from the cavity is κ.

A THREE-LEVEL ATOM MODEL

For the model, we consider a solid-state system with a well defined and isolated lowest energy optical transition and a manifold of higher energy states that when populated, relax incoherently to the lowest energy state. This system is representative of many types of solid-state quantum dot as well as various other systems that can be found in the solid state. For the purposes of the model, the system is simplified as a three-level ladder system, with the upper level being the pumping level, which relaxes incoherently to the middle level, which in turn relaxes to the ground state with the emission of a photon. All the relevant details of this system are depicted in Fig. 1, where we have indicated that the upper state is usually one in a manifold of states. The excitation sequence proceeds as follows: The transition from the ground state to the upper level is driven coherently with a short pulse. The system then incoherently relaxes down to the middle state. The transition from the middle state to the ground state is via emission of a photon. The Stark tuning field acts on the middle level in order to bring the optical transition into resonance with a single optical cavity resonance. If the optical cavity mode has both a low mode volume and a high Q, the regime of strong-coupling cavity quantum electrodynamics can be approached. In terms of the model, this cavity enhancement of the emission process is contained in the coupling frequency of the interaction g. Therefore it is useful to normalize the essential model parameters against g. The basic Hamiltonian for the system is

$$\hat{H}/\hbar = \omega\hat{a}^\dagger\hat{a} + \sum_{j=1}^{3}[\omega_j + A_j(t)]|j\rangle\langle j| + ig(\hat{a}|2\rangle\langle 1| - \text{H.c.})$$

$$+ \Omega(t)\cos(\omega_{31}t)(|3\rangle\langle 1| + \text{H.c.}), \quad (1)$$

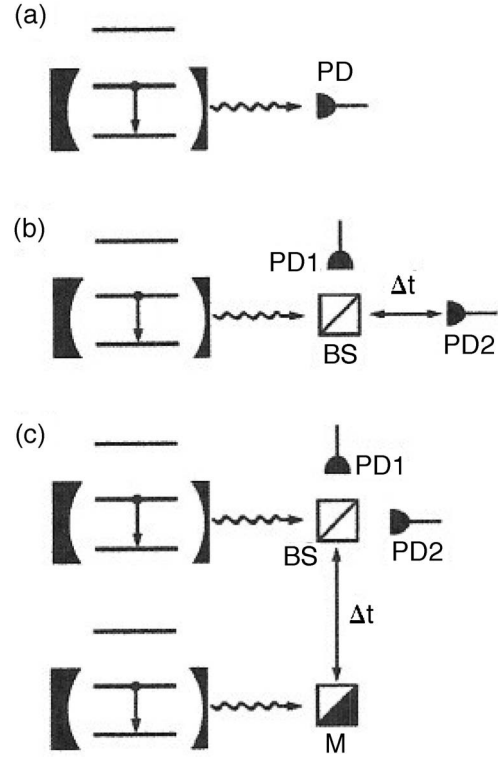where $\hat{a}$ is the annihilation operators for the cavity field

FIG. 2. Schematic diagrams of the three experiments that are simulated: (a) Direct photodetection with a photon counting photodetector (PD). (b) Detection of the second-order correlation function $g^{(2)}(\Delta t)$. The elements of the experiment are a 50/50 beam splitter (BS) and two photon counting photodetectors (PD1 and PD2). The variable time delay is also indicated. (c) The Hong-Ou-Mandel (HOM) interference experiment involving two single-photon sources, a mirror (M), 50/50 beam splitter (BS), and two photon counting photodetectors (PD1 and PD2).

mode which has a frequency ω. The atomic operators are expressed in terms of projection operators with the energies of the three levels given by ω_j for $j=1,2,3$. They also have a time dependence represented by the $A_j(t)$ terms, which are used to represent the Stark tuning of the atomic energy levels. The coupling of the lowest transition to the cavity mode is represented by the parameter g. The last term represents a coherent driving pulse, with $\Omega(t)$ the time-dependent pulse amplitude. In this model the atomic levels $|3\rangle$ and $|2\rangle$ are only coupled incoherently. This means that any coherent dynamics of the upper level are completely decoupled from the lower levels and all the physics is contained in the relaxation rate to populate the middle level. In order to simplify the system for efficient numerical simulation and highlight the relevant dynamics, we rewrite the Hamiltonian in the interaction picture and make the rotating wave approximation. Thus the Hamiltonian reduces to the following form:

$$\hat{H}/\hbar = A(t)\hat{\sigma}_z^{21} + \Omega(t)(\hat{\sigma}_+^{31} + \text{H.c.}) + ig(\hat{a}\hat{\sigma}_+^{21} - \text{H.c.}), \quad (2)$$

where we have used Pauli operator notation for the atomic transitions with the superscripts referring to the two levels that each operator acts upon. The first two terms are the

time-dependent Stark pulse and coherent driving pulse term, respectively.

We include the loss terms in the standard manner with the following master equation in Linblad form:

$$L = \frac{1}{i}[\hat{H}, \hat{\rho}] + \sum_{l=1}^{3} \hat{C}_l \hat{\rho} \hat{C}_l^\dagger - \frac{1}{2}(\hat{C}_l^\dagger \hat{C}_l \hat{\rho} + \hat{\rho} \hat{C}_l^\dagger \hat{C}_l), \quad (3)$$

where $\hat{H}$ is the Hamiltonian described above and $\hat{\rho}$ is the reduced density operator. The loss terms, $\hat{C}_1 = \sqrt{\kappa} \hat{a}$, $\hat{C}_2 = \sqrt{\gamma_{21}} \hat{\sigma}_-^{21}$, and $\hat{C}_3 = \sqrt{\gamma_{32}} \hat{\sigma}_-^{32}$, represent the coupling of the cavity mode to other modes outside the cavity, the spontaneous emission from the $\hat{\sigma}_+^{21}$ transition with decay rate γ_{21}, and the incoherent population of level $|2\rangle$ with a rate γ_{32} following the pump pulse.

SIMULATIONS

In order to simulate a variety of different experiments, including the Hong-Ou-Mandel interferometer, we use a quantum trajectory approach. This gives us great flexibility in choosing different detection schemes that comprise the different experiments. Direct numerical integration of the master equation was also employed to check the quantum trajectory results. One difficulty with the simulation is the vastly different time scales involved. In order to simulate femtosecond pulse excitation and subsequent coherent interactions on a nanosecond or longer time scale, it would be necessary to use a very large amount of time steps. However, we note that excitation with a femtosecond pulse is equivalent to a δ-function population of the upper excited state on the coherent atom-cavity interaction time scale. Therefore it is sufficient to simply start the atom in the excited state, rather than use the coherent driving term $\Omega(t)$. On the other

hand, in order to simulate a pulse train, a driving term is required. We accomplished this by using a coherent Gaussian pulse envelope $\Omega(t)$ to invert the population (i.e., a π pulse), while suppressing the relaxation term γ_{32} during the pulse period. After the pulse had populated the upper state, the relaxation was turned on. This allows the use of longer pump pulses compatible with the time scales needed for the simulation and effectively simulates δ-function population of the upper state. This was confirmed by comparing results using either an initially populated excited state or the coherent pulsed population with switched upper state relaxation. In both cases, the simulation converged to the same result.

Three different experiments were simulated, as depicted in Fig. 2. The first is direct photodetection, which displays the probability of detecting a photon per time interval. This experiment shows the pulse train that is used in subsequent experiments. The next experiment is a Hanbury-Brown-Twiss experiment to detect the second-order correlation function $g^{(2)}(\tau)$, defined as

$$g^{(2)}(\tau) = \frac{\langle \hat{a}^\dagger(t) \hat{a}^\dagger(t+\tau) \hat{a}(t+\tau) \hat{a}(t) \rangle}{\langle \hat{a}^\dagger(t) \hat{a}(t) \rangle^2}. \quad (4)$$

This experiment is used to ensure that the simulation is actually producing single photons. The third experiment is a Hong-Ou-Mandel interferometer. This simulation involves simulating two independent single-photon sources and combining their outputs with a beam splitter and looking at the joint detection probabilities as a function of differing temporal displacements of one source from the other. We are at liberty to express our results in a number of ways. Rather than using the number of coincidence counts directly, we choose to express the interference results in terms of a HOM visibility, defined as

$$\text{HOM}_{vis} = 1 - \frac{[P(PD1, PD1) + P(PD2, PD2) - P(PD1, PD2) - P(PD2, PD1)]}{[P(PD1, PD1) + P(PD2, PD2) + P(PD1, PD2) + P(PD2, PD1)]}, \quad (5)$$

where the various $P(PDi, PDj)$ correspond to the joint photodetection probability with photons detected at the photodetectors corresponding to their respective index. Such a quantity is in general not possible with current photodetector technology, but is in principle possible.

For all simulations a truncated Fock space was used for the cavity mode. The truncation was made at either $n=3$ or $n=4$ to allow for the possibility of multiple-photon occupation and thus ensuring that the second-order correlation function $g^{(2)}(\tau)$ is a meaningful test for single-photon emission.

The simulations are conducted for each of two cases, which we refer to as the active source and the passive source. The active source is the one where the atom is kept off resonant for a time sufficiently long to allow efficient relaxation

of the upper excited state to the intermediate level with high probability. The atom is then brought into resonance with the cavity for a time long enough to transfer the excitation into the cavity mode (a π pulse) after which it is again rapidly detuned, leaving the excitation in the cavity. The passive source is the case in which a Stark tuning voltage may be applied to bring the atom permanently into resonance with the cavity. This is the usual case for cavity enhanced single-photon sources.

The efficiencies of each single-photon source are also determined and compared. This was conducted using both the quantum trajectory simulations and direct integration of the master equation. With the quantum trajectory simulations, the emission efficiency was simply estimated by counting all
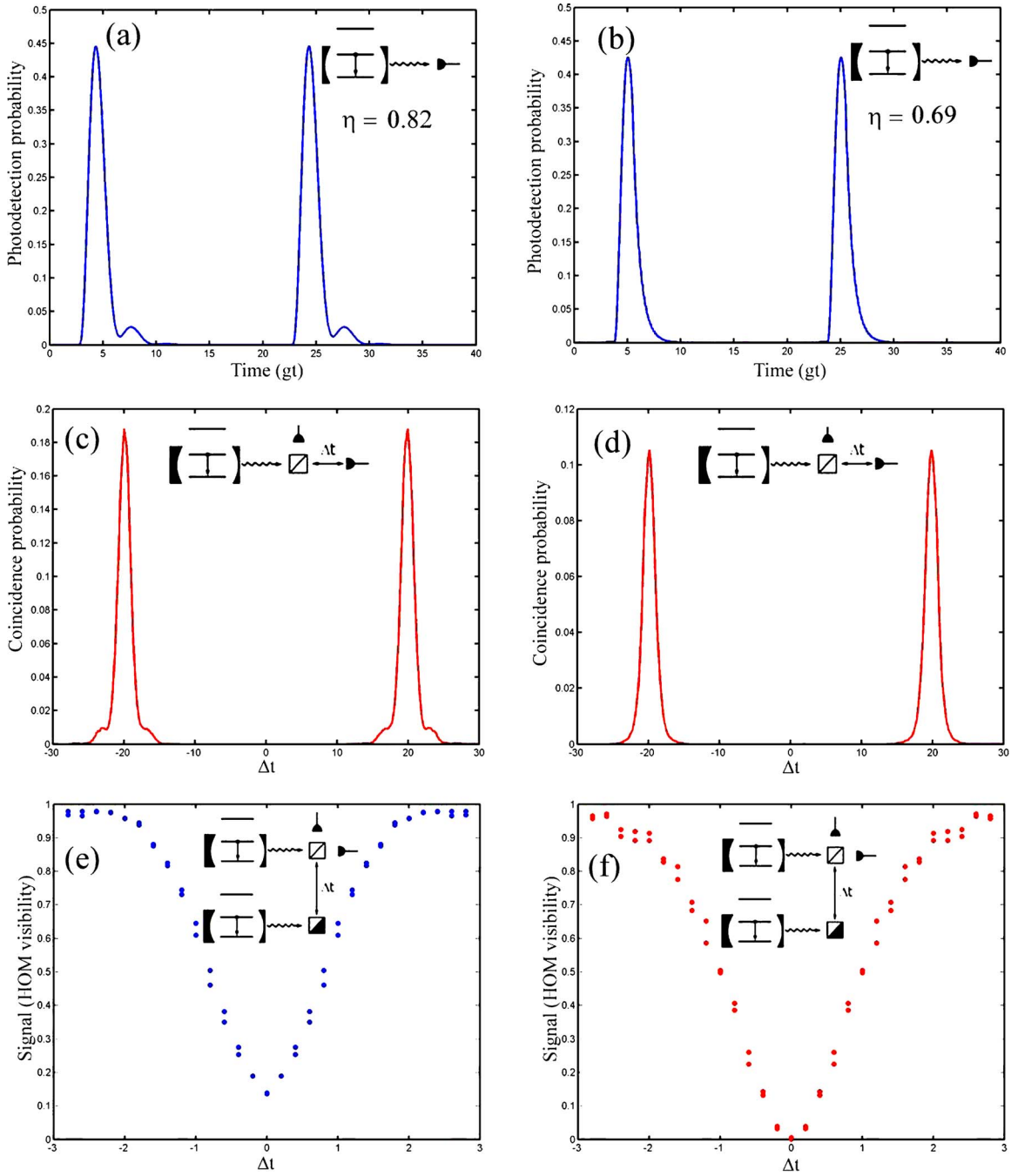
FIG. 3. (Color online) Comparison between a passive single-photon source and an actively switched single-photon source for the case of operation in the strong Purcell regime ($\kappa/g=1.5$, $\gamma_{21}/g=0.2$). Direct photodetection is shown in (a) and (b) representing two successive pulses from the passive and active sources, respectively. The efficiency of photon emission (η) is given in each figure. Antibunching is observed in the suppression of the $\Delta t=0$ peak for both sources in (c) and (d). The HOM interference (Eq. (5)) is shown for the passive and active source in (e) and (f), respectively.

the photon detection events, which correspond to the cases where a quantum jump occurs due to photon emission. These numbers were ratioed with the number of trajectories and compared to the case of pure cavity emission in order to provide proper normalization. With the master equation simulations, the efficiency was calculated by integrating the pulse envelope to determine the total probability for detecting a photon with each pulse. Both cases yielded equivalent estimates of the efficiency.

RESULTS

We first investigate the more conventional regime for single-photon sources: the so-called strong Purcell regime. In this regime it is usual to operate with $g < \kappa$ which defines the bad cavity case. This case provides efficient generation of single photons output via the cavity mode and is therefore highly pertinent to single-photon sources. We set the system parameters as $g=1$, $\kappa=1.5$, $\gamma_{21}=0.2$, and $\gamma_{32}=3$. The single-
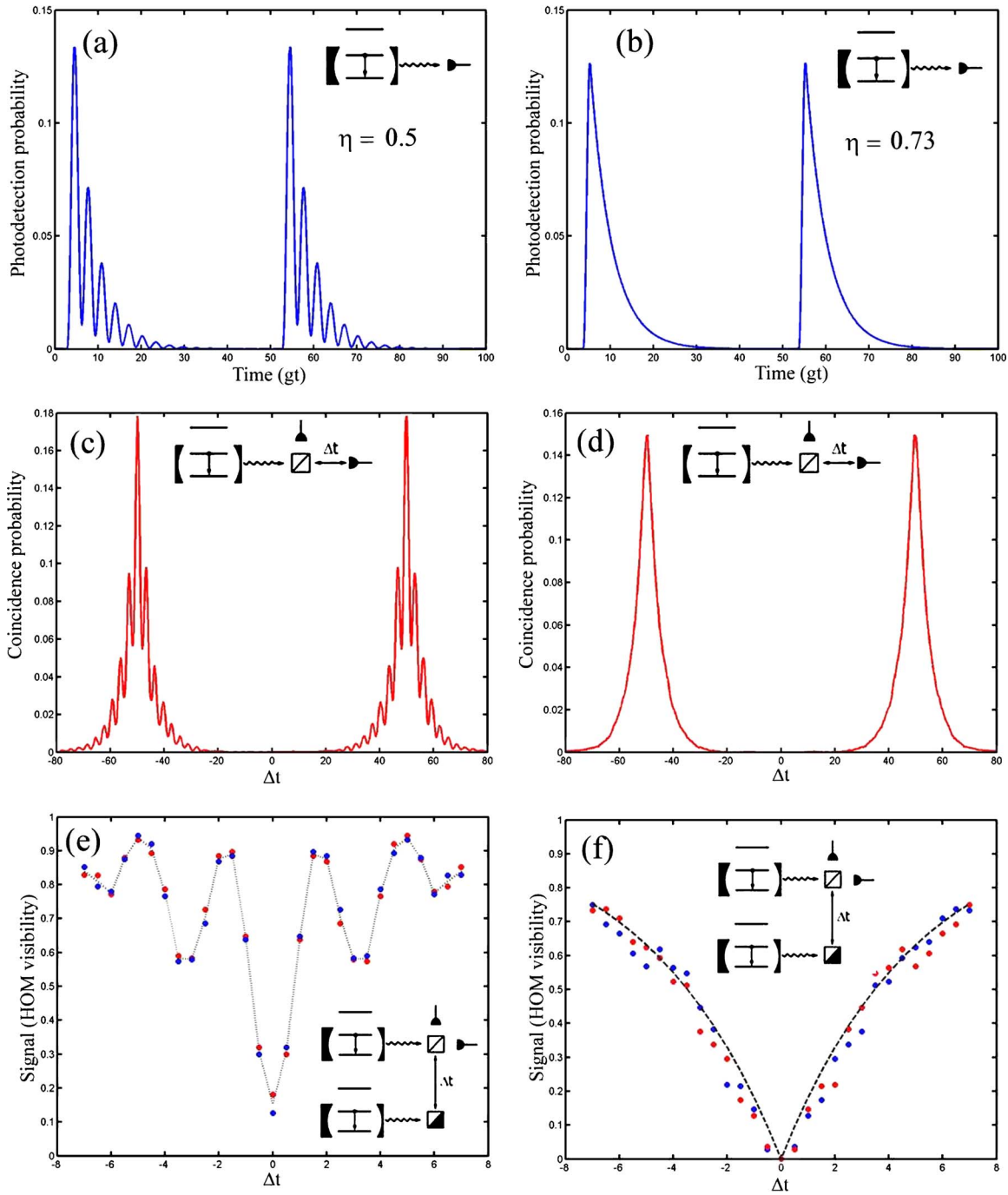
FIG. 4. (Color online) Comparison between a passive single-photon source and an actively switched single-photon source for the case of operation in the strong-coupling regime ($\kappa/g=0.2$, $\gamma_{21}/g=0.2$). Direct photodetection is shown in (a) and (b) representing two successive pulses from the passive and active sources, respectively. The efficiency of photon emission (η) is given in each figure. Antibunching is observed in the suppression of the $\Delta t=0$ peak for both sources in (c) and (d). The HOM interference (Eq. (5)) is shown for the passive and active source in (e) and (f), respectively. The dotted line in (e) is provided as a guide to the eye. A fit corresponding to pure exponential decay (dashed line) is included in (f).

photon pulses resulting from two successive pump pulses are shown in Figs. 3(a) and 3(b) for both the active and passive cases. The passive case has the highest efficiency at η =82% and the pulse shape exhibits some slight oscillation due to the coupling between the atom and cavity. In contrast, the active case shows purely exponential decay, characteristic of the cavity, while it has a slightly lower efficiency of

69%. The second-order correlation functions shown in Figs. 3(c) and 3(d) show clear antibunching via the suppression of the correlation at $\tau=0$. While the differences in pulse shape seem only marginal in this regime, we see in Figs. 3(e) and 3(f) that the HOM dip is not complete in the passive case, whereas complete nonclassical interference can be restored if active switching is employed.

In the strong-coupling regime $(g > \gamma_{21}, \kappa)$, resonant behavior exhibits vacuum Rabi oscillations and the cavity output deviates from the bare cavity exponential decay. In this regime efficient single-photon sources require $\kappa/\gamma_{21} > 1$ in order to achieve high efficiency output via the cavity mode. However, it is possible to achieve similar efficiencies for loss ratios less than 1 by actively switching the atom detuning into resonance for a time sufficient to allow half a Rabi cycle (i.e., a π pulse). To illustrate this we choose to simulate the case of a loss ratio of $\kappa/\gamma_{21} = 1$, and set the system parameters as $g = 1$, $\kappa = \gamma_{21} = 0.2$, and $\gamma_{32} = 3$. The single-photon pulse envelopes resulting from two successive pump pulses are shown in Figs. 4(a) and 4(b) for the active case (a) and passive case (b). Here we see that the passive case displays clear vacuum Rabi oscillations and attains a limiting efficiency of 50%, whereas by actively switching the detuning into and out of resonance we are able to regain pure cavity exponential decay and attain an efficiency of 73%, which exceeds the theoretical efficiency for the passive case [21]. The respective second-order correlation functions $g^{(2)}(\tau)$ are shown in Figs. 4(c) and 4(d), where we see that both sources display clear antibunching behavior in the suppression of the correlation around $\tau = 0$, characteristic of a good single-photon source. Finally the nonclassical interference experiment is simulated in Figs. 4(e) and 4(f). Here we see that the passive case does not show a complete interference dip, whereas in the active case we are able to regain complete nonclassical interference. Therefore by using an active single-photon source, we are able to provide an efficient source of indistinguishable single photons in the strong-coupling regime. Such a technique could overcome the constrains on efficient single-photon sources in this regime.

In the above simulations we have delayed the switching pulse by $gt = 1$ in order to suppress stochastic timing jitter in populating the level $|2\rangle$. This time delay was chosen such that the HOM visibility was greater than 99.9%. Higher emission efficiencies are possible if shorter delays are used, but at the expense of the HOM visibility. This complementary behavior of the HOM visibility and the emission efficiency is a generic property. However, the magnitude of the effect is entirely dependent on the system parameters. As an example we look at the regime $g = 1$, $\kappa = 2.5$, $\gamma_{21} = 0.2$, and $\gamma_{32} = 3$. This is further into the Purcell regime where the cavity loss completely dominates the coherent atom-cavity interaction, and was chosen so that the trailing edge of the Stark tuning pulse does not affect the single-photon pulse envelope (i.e., the switch on delay entirely determines the resultant pulse properties). Operation in this regime is thus useful for examining the effect of the delay of the Stark tuning pulse on both the emission efficiency and HOM visibility. This is plotted in Fig. 5. We find the efficiency starts from that of the passively resonant case (i.e., the efficiency achieved without Stark tuning) at around 82% and progressively lowers with increasing delay, while the HOM visibility starts from that attained with the passively resonant case of 85% and approaches unity with increasing delay. Therefore the efficiency of the single-photon source and the HOM visibility are essentially complementary qualities and cannot both be maximized, although both high efficiency and near perfect HOM visibility could be attained with an appropriate source.
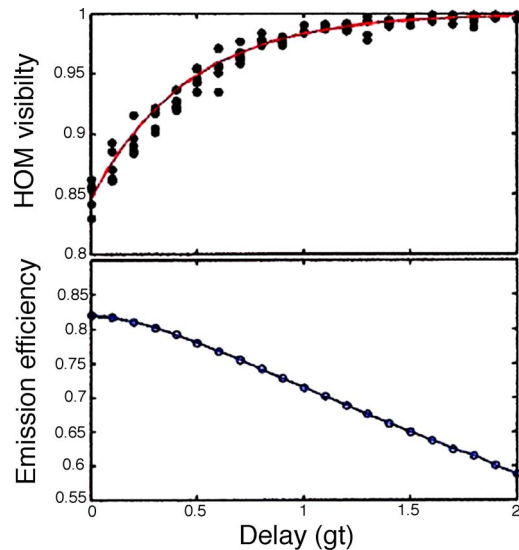

FIG. 5. (Color online) The dependence of both the HOM visibility and photon emission efficiency on the delay between the pump pulse and the leading edge of the active Stark tuning pulse (the line in the HOM visibility plot is simply a guide to the eye). The simulations were conducted in the Purcell regime ($\kappa/g = 2.5$, $\gamma_{21}/g = 0.2$) where coherent cavity dynamics no longer affect the pulse shape.

PULSE SHAPING

The use of a Stark tuning pulse to control the quantum dynamics of a cavity QED system brings with it the possibility of more advanced control of the interaction in order to tailor the pulse envelope to the particular application. Such an ability would be beneficial for certain schemes such as photon quantum memories, where a single-photon pulse can be stored in the collective coherent behavior of an atomic gas [8,9], for example. For such applications, symmetric pulse envelopes are desirable, rather than the decaying exponential that characterizes pure cavity decay. Furthermore, it has been theoretically shown that symmetric Gaussian pulses are optimal for robust quantum information processing [22].

In general, the dynamics of the Stark tuned cavity QED system are complex and highly nonlinear, however, it may still be possible to arbitrarily tailor the wave packet using feedback to a learning algorithm. Here we provide a concrete example of the possibility for pulse shaping by arbitrarily choosing the Stark tuning pulse to be highly asymmetric in time in the opposite sense to the output pulse. The naive reasoning behind this is to slowly bring the atom into resonance so that the cavity output slowly builds to a maximum before decaying.

In Figs. 6(a) and 6(b) we show both the conventional switching Stark pulse and the asymmetric slow turn-on pulse, respectively. The respective single-photon pulse envelopes are shown in Figs. 6(c) and 6(d). Here we find that a relatively simple Stark tuning pulse can readily produce a very symmetric output pulse envelope. In fact we have fitted the pulse envelope in Fig. 6(d) with a Gaussian and find a remarkably close fit. This demonstrates the ability to tailor the wave packets using a Stark tuning control voltage. Fur-
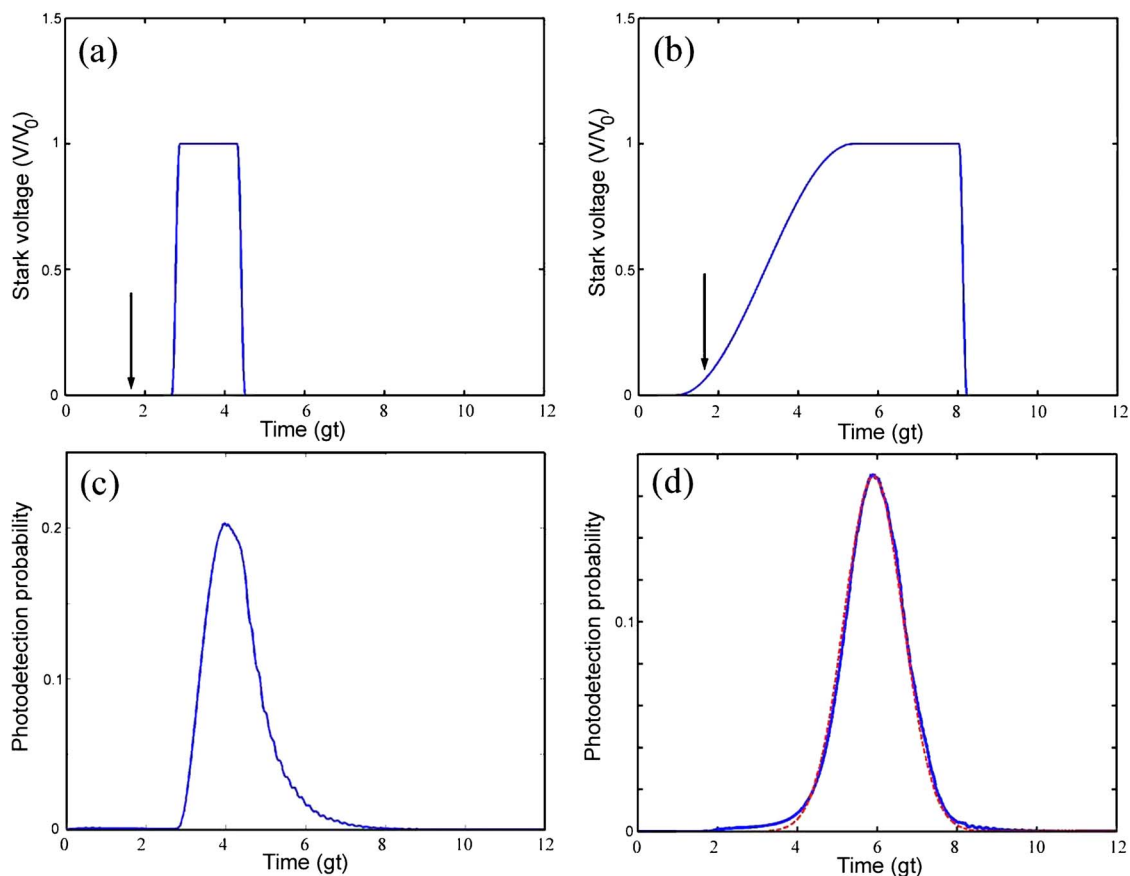
FIG. 6. (Color online) An example of simple pulse shaping via an asymmetric Stark tuning pulse. The standard Stark tuning pulse is shown in (a) and the asymmetric Stark tuning pulse used for pulse shaping is shown in (b). The arrows indicate the position of the pump pulse $\Omega(t)$. The resultant pulse envelopes are shown in (c) and (d) for operation in the strong Purcell regime of $\kappa/g = 1.5$, $\gamma_{21}/g = 0.2$. A Gaussian fit is included in (d) (dotted line).

thermore, it seems that the very desirable Gaussian pulses [22] may be made with relatively simple Stark tuning pulse envelopes.

By using the asymmetric tuning pulse we find that the efficiency of photon emission via the cavity mode is reduced from 67% to 40%. While this is still respectable, it is entirely dependent on the system parameters. For example, if an atomic relaxation rate, $\gamma_{21} = 0.02$ is used, the efficiency is dramatically improved to 86%. Therefore the ability to pulse shape with high efficiency puts added constraints on the system. Nevertheless, realistic systems, such as ion dopants in crystal matrices, could possibly meet these requirements.

DISCUSSION

The efficiency of the single-photon sources can approach unity in many solid-state systems. By imposing the additional constraint that the system relax to the lowest excited state (the upper state of the relevant two-level transition) before tuning the transition into resonance with the cavity, the efficiency of photon emission from the cavity can suffer. In order for this technique to be effective and useful, the major constraint on the solid-state system is that decoherence rate of the upper state, γ^ϕ, be much less than the coupling frequency g. For a lifetime limited transition, $\gamma^\phi = \gamma_{21}$. In our

simulations we have taken $\gamma_{21}/g = 0.2$ and find we are able to generate single photons with the active scheme comparable to the passive scheme. Moreover, the active scheme is more flexible in that it can efficiently generate single photons with both good and bad cavities. These constraints are more important where pulse shaping is concerned. In our simulations, we found the efficiency of generating shaped pulse noticeably dropped compared to both the standard active scheme and the passive scheme. Therefore systems with long decoherence times are more likely to provide sources capable of active pulse shaping. Such systems could comprise rare-earth dopants, which typically have extremely narrow homogeneous linewidths [23].

The technique of using Stark tuning to improve on the performance of single-photon sources should be applicable to a variety of different materials and cavity geometries. The main constraint is the ability to shift the detuning of the atom-cavity system sufficiently quickly in order to effectively control the interaction dynamics. This time scale is then set by the dynamics of the system such as the vacuum Rabi frequency as well as the atomic decay and pure dephasing rates. The remaining constraint is the ability to Stark tune the atomic resonance with realistic voltages over a range at least ten times the vacuum Rabi frequency.

Fortunately, in the solid state there are many possibilities for suitable atomlike emitters. For example, the NV^- center

in diamond has a lifetime of the order of 10 ns and is widely Stark tunable [24]. In fact, Stark tuning of single NV^- centers has recently been proposed as a method for actively Q switching photonic-band-gap cavities [25]. If such an emitter were used with a fused silica microsphere resonator, vacuum Rabi frequencies of around 500 MHz are possible. This allows for the use of readily available GHz electronics to provide the Stark tuning voltage. Such a system would also be amenable to pulse shaping, such as we have described above.

There are many other possibilities for suitable Stark tunable solid-state emitters, including various color centers [24], single-ion dopants [26], single molecules [27], and single quantum dots and nanocrystals [28]. Furthermore, the properties of many of these emitters can be modified by effects such as dielectric screening, which can reduce the effective oscillator strength of a transition where appropriate [29]. On the other hand, microcavities with exceedingly small mode volumes, such as those that can be made with photonic-band-gap materials, could be used to significantly enhance the oscillator strength of single rare-earth dopants, which otherwise have very promising properties.

The main problem with current solid-state sources is the timing jitter induced by incoherent population of the upper state of a transition [7]. The use of Stark tuning overcomes this by waiting for a period long enough for most of the population to relax to the upper state of the transition before the transition is brought into resonance with the cavity. This process is itself susceptible to timing jitter. Therefore if our proposed scheme is to provide any benefit, the timing of the electronics must be stable enough to substantially reduce the timing jitter of the system. Currently, electronics are able to provide timing accuracy at the picosecond level. This is still more than two orders of magnitude longer than the time scale set by interference, but is shorter than many relaxation processes in the solid state and so is likely to improve the photons' indistinguishability. In fact, the relevant time scale for HOM interferometry is the relaxation time of the cavity. This means current electronic technology can potentially provide significant improvement in HOM interference or photon indistinguishability, which should be in the order of that which is presented in this paper.

CONCLUSION

We have investigated the use of Stark tuning of an arbitrary emitting transition in a solid-state system in order to gain control of the interaction between emitter and a high-Q optical cavity resonance. Quantum trajectory simulations have been used to model the operation of the system as well as model the detection scheme, which includes photon correlation experiments and the two-photon Hong-Ou-Mandel interference experiment. We have shown that it is possible, using well timed Stark tuning pulses, to remove the timing jitter that results from stochastic pumping of the emitting transition. This results in complete recovery of the Hong-Ou-Mandel interference. Furthermore, we have demonstrated that simple modification of the Stark tuning pulse shape allows shaping of the photon wave packet from decaying exponential to a symmetrical Gaussian wave packet. More complex control of the photon wave packet is in principle possible if more complex procedures are employed, such as the use of adaptive algorithms. It has also been shown that the symmetrical wave packets still display complete HOM interference.

The procedure for effective Stark tuning control of a solid-state source depends on the material parameters. Both the decoherence time and transition strength need to be suitable for effective Stark tuning control of the interaction. It is expected that such a source is within the technological possibilities of nanocrystal emitters as well as various color centers.

The ability to provide a solid-state single-photon source which is able to provide indistinguishable photons on demand would be extremely useful for all optical quantum computing schemes. Furthermore, the ability to shape the photon wave packet would make it also suitable for use in various photon memories that have been proposed. Therefore this technology promises a compact solid-state single-photon source with an unprecedented degree of control over the photon wave packets.

[1] E. Knill, R. Laflamme, and G. J. Milburn, Nature (London) **409**, 46 (2001).

[2] J. L. O'Brien, G. J. Pryde, A. G. White, T. C. Ralph, and D. Branning, Nature (London) **426**, 264 (2003).

[3] T. B. Pittman, M. J. Fitch, B. C. Jacobs, and J. D. Franson, Phys. Rev. A **68**, 032316 (2003).

[4] S. Gasparoni, J. W. Pan, P. Walther, T. Rudolph, and A. Zeilinger, Phys. Rev. Lett. **93**, 020504 (2004).

[5] T. C. Ralph, Rep. Prog. Phys. **69**, 853 (2006).

[6] C. K. Hong, Z. Y. Ou, and L. Mandel, Phys. Rev. Lett. **59**, 2044 (1987).

[7] A. Kiraz, M. Atature, and A. Imamoglu, Phys. Rev. A **69**, 032305 (2004).

[8] T. Chaneliere, D. N. Matsukevich, S. D. Jenkins, S.-Y. Lan, T. A. B. Kennedy, and A. Kuzmich, Nature (London) **43**, 833 (2005).

[9] C. W. Chou, S. V. Polyakov, A. Kuzmich, and H. J. Kimble, Phys. Rev. Lett. **92**, 213601 (2004).

[10] J. McKeever, A. Boca, A. D. Boozer, R. Miller, J. R. Buck, A. Kuzmich, and H. J. Kimble, Science **303**, 1992 (2004).

[11] B. Darquie, M. P. Jones, J. Dinjan, J. Beugnon, S. Bergamini, Y. Sortais, G. Messin, A. Browaeys, and P. Grangier, Science **309**, 454 (2005).

[12] A. Kuhn, M. Hennrich, T. Bondo, and G. Rempe, Appl. Phys. B: Lasers Opt. **69**, 373 (1999).

[13] M. Keller, B. Lange, K. Hayasaka, W. Lange, and H. Walther, Nature (London) **431**, 1075 (2005).

[14] J. K. Thompson, J. Simon, H. Loh, and V. Vuletic, Science **313**, 74 (2006).

[15] C. Santori, D. Fattal, J. Vucković, G. S. Solomon, and Y.

Yamamoto, Nature (London) **419**, 594 (2002).

[16] C. Santori, D. Fattal, J. Vucković, G. S. Solomon, and Y. Yamamoto, Fortschr. Phys. **52**, 1180 (2004).

[17] P. Michler, A. Kiraz, C. Becher, W. V. Schoenfeld, P. M. Petroff, L. Zhang, E. Hu, and A. Imamoglu, Science **290**, 2282 (2000).

[18] A. Beveratos, S. Kuhn, R. Brouri, T. Gacoin, J.-P. Poizat, and P. Grangier, Eur. Phys. J. D **18**, 191 (2002).

[19] C. Kurtsiefer, S. Mayer, P. Zarda, and H. Weinfurter, Phys. Rev. Lett. **85**, 290 (2000).

[20] J. Vucković, D. Englund, D. Fattal, E. Waks, and Y. Yamamoto, Physica E (Amsterdam) (Amsterdam) **32**, 466 (2006).

[21] G. Cui and M. G. Raymer, Opt. Express **13**, 9660 (2005).

[22] P. P. Rohde, T. C. Ralph, and M. A. Nielson, Phys. Rev. A **72**, 052332 (2005).

[23] Y. Sun, C. W. Thiel, R. L. Cone, R. W. Equall, and R. L. Hutcheson, J. Lumin. **98**, 281 (2002).

[24] D. Redman, S. Brown, and S. C. Rand, J. Opt. Soc. Am. B **9**, 768 (1992).

[25] A. D. Greentree, J. Salzman, S. Prawer, and L. C. L. Hollenberg, Phys. Rev. A **73**, 013818 (2006).

[26] A. L. Alexander, J. J. Longdell, M. J. Sellars, and N. B. Manson, Phys. Rev. Lett. **96**, 043602 (2006).

[27] Ch. Brunel, Ph. Tamarat, B. Lounis, J. C. Woehl, and M. Orrit, J. Phys. Chem. A **103**, 2429 (1999).

[28] S. A. Empedocles and M. G. Bawendi, Science **278**, 2114 (1997).

[29] B. Wehrenberg, C. Wang, and P. Guyot-Sionnest, J. Phys. Chem. B **106**, 10634 (2002).